Electronic Supplementary Information

The Novel Hydrogen-Rich Binuclear Cobalt Complex Anion, $[(CoH_3)_2H_3]^{5-}$

Donald Linn[a]*, Jerod Kieser[a] and, Jason Shearer[b]*

[a] *Department of Chemistry, Indiana University Purdue University Fort Wayne, 2101 Coliseum Blvd. E., Fort Wayne , IN, US. Fax: 260-481-6070 Tel: 260-481-6070; E-mail: linn@ipfw.edu*

[b] *Department of Chemistry, University of Nevada, Reno, NV, US. Fax: 775-784-6804 Tel: 775-784-7785; E-mail: shearer@unr.edu*

Table of Contents **Page**

More details on data collection and analysis

General:

The details have been reported previously concerning the purification of solvents and the use of vacuum line and argon-filled glove box to handle samples.[1] The use of a hydrogen uptake apparatus was also reported elsewhere.[2] Further the NMR operated a 200 MHz (Varian/Agilent) at ambient temperature and data collection used a one pulse sequence for 64 transients, with flip angle 30°, 10 kHz sweep width, 5 s delay, and 2.5 s acquisition time. The data was zero filled to 32k data points and processed using ACD software on a PC.[3] The IR data were acquired on Nicolet Magna spectrometer with DTGS detector using either NaCl (Nujol) windows collecting 32 transients at a resolution of 4 cm^{-1}.

An EPR spectrum of (**1**) diluted in boron nitride was obtained on a Bruker EMX^{plus} EPR operating at 10 K over the course of 60 h (nu = 9.12 GHz, amplitude modulation = 5.0 G, microwave power = 20 mW, field range 250 - 6000 G).

In order to determine bromide and magnesium content by titrimetric analyses it was necessary to remove the interfering cobalt. This was accomplished by hydrolysis of 10-20 mg samples of (**1**) using 0.1 M acetate pH 6 buffer, followed by magnetic separation of the resulting cobalt oxide (presumably Co_3O_4) using a small SmCo wafer magnet. The resulting supernatant layer was syringe filtered through a 0.2 μm PTFE membrane. The bromide analysis was by the Mohr method and the magnesium was obtained by a complex-formation (EDTA) titration.[4] Each analysis were performed in triplicate.

Cobalt was determined based on multiple (four) samples using a spectrometric method for cobalt which was analyzed by a spectrophotometer (HP 8453) with the accompanying software, where routine calibrations determined the concentration of $[CoCl_4]^{4-}$ [λ_{max} = 692 nm; ε_{max} ~ 570 L mol^{-1} cm^{-1} (11 M HCl)].

Hydrolysis experiments to measure hydridic hydrogen content on small solid samples (**Table 1**) were performed using a micro-syringe and computed using gas law equations. The total pressure was corrected for the vapor pressure for THF (Antoine equation) and the water.[5] The small

amount of toluene vapor and solubility of hydrogen were neglected. The equilibration of the gas volumes were for two minutes, during which time the volume remained constant, and thus the equilibration between the gas, liquid and solid phases was judged to be slow and negligible. Estimation for the uncertainty in THF due to its water solubility and interactions with metal ions was estimated to result in a concentration perhaps 10% too low.

XAS Data Collection:

In a glovebox samples were finely ground in Nujol, and placed in aluminum sample holders between windows made from Kapton tape providing for a 1.0 mm pathlength. Final solid-solution concentrations were 0.9 M in cobalt (optimal sample thickness 0.96 mm for a 1.5 edge jump calculated using McMaster coefficients). The sample holders were then slowly frozen in liquid such that the Nujol did not ice or crack making for a homogeneous sample. Data were then collected on beamline X3b at the National Synchrotron Light Source (Brookhaven National Laboratories) employing a Si 111 double-crystal monochromator and a low angle Ni mirror for harmonic rejection. Samples were maintained at 25 K using a closed-cycle helium Displex cryostat. Data were collected in transmission mode using dinitrogen filled ionization chambers (100 kHz rep rates). Calibration spectra of Co-foil were measured simultaneously with the XAS data (first inflection point set to 7709.5 eV). Data were collected in 5 eV steps in the pre-edge region (1 s integration time; 7509 – 7689 eV), 0.3 eV steps in the edge region (3 s integration time; 7689 – 7729 eV), 1 eV steps in the near edge region (3 s integration time; 7729 – 7859 eV), 2 eV steps in the far edge region (5 s integration time; 7859 – 8109 eV) and 5 eV steps from 8109 eV – 8810 eV (5 s integration time). The presented data represents the summed average of 20 individual data sets. Data were of high quality out to at least $k = 15$ Å^{-1}.

Co K-edge XAS Data Analysis and EXAFS Simulations:

Data were analyzed using *EXAFS123* as previously described.[6,7] Briefly, individual spectra were inspected prior to averaging. Baseline fitting and determination of the edge-height was accomplished by fitting the data from 7509 to 8441 eV (except for the data between 7724 to 7738 eV, which was difficult to simulate). A four-region cubic spline was fit simultaneously with the pre-edge, edge, and EXAFS parameters. The edge was modeled as an integral of a pseudo-Voigt function (75% Gaussian + 25% Lorentzian peaks) while the pre-edge peaks were modeled as simple sums of Gaussian and Lorentzian peaks (1:1). Two pre-edge peaks were obtained at 7714.57(3) eV (width = 1.64(1) eV, height = 0.026(5) % edge height) and 7719.82(1) eV (width = 2.07(1) eV, height = 0.39(1) % edge height).

EXAFS data were simulated using the single-scattering approximation:

$$\chi_{calc} = \sum_{i=1}^{\text{no.ofshells}} n_i f_i k_1^{-1} R_i^{-2} \exp(-2\sigma^2 k_i^2) \sin(2k_i R_i + \alpha_i)$$

where the Debye-Waller factor σ_i is defined as:

$$\sigma_i^2 = \langle (r_i - R_i)^2 \rangle$$

and:

$$k_i = [2m_e(E - (7725 + \Delta E))]^{1/2}/\hbar$$

where ΔE (–0.38 eV) is an adjustable parameter to reflect the difference between the true ionization energy of the Co K-electron and 7725 eV. This parameter was allowed to freely float on the first set of refinements and then restrained to that initial value throughout the simulations. All other parameters have their typical meaning

Phase (α_i) and amplitude (f_i) functions for Co-Co, Co-H, Co-Br and Co-Mg single scattering pathways were reconstructed using FEFF 9.0[8] in an identical manner as outlined in detail before.[7b,c] The Co compounds compounds that were utilized in the construction of phase and amplitude functions were the DFT generated models from below. Additional Mg-Br units were placed about the Co dimers. Co-scatterer bond lengths were systematically varied to bracket the predicted bond-length (± 1.0 Å from predicted length in 0.05 Å steps).

All EXAFS simulations are based on unfiltered $k^3(\chi)$ spectra, with data analyzed from 2.0 to 15.0 $Å^{-1}$. The Co-Co scatter number was restrained to 1 and all other parameters allowed to freely refine. The data were modeled by progressively adding shells to the simulations and subsequent evaluation of the error parameter ε^2:

$$\epsilon^2 = [n_{idp}/(n_{idp} - n_p)] \times \text{average } [(y_{data} - y_{calc})/\sigma_{data}]^2$$

where n_{ida} are the number of experimental data points, n_p are the number of parameters refined in the simulation ($y_{data} - y_{calc}$) and σ_i is the estimated uncertainty in the data.[7b,c] Although ε^2 progressively

lowered upon the addition of subsequent shells, all simulations to the data must be considered valid as the error parameter varied between 0.82 – 0.68 from the Co-Co only model to the model including Co, H, Mg and Br scatterers.

DFT Analysis:

Electronic structure calculations were performed using the DFT and *Ab Initio* Software package ORCA v. 2.9.[9] All calculations employed the mPWPW91 hybrid density functional, the aug-def2-TZVPP basis set and the Broken-Symmetry formalism. Default ORCA geometry optimization and SCF cutoffs were used on the geometry optimizations. Cobalt dimers with between 9 - 14 hydrides were considered. Of the six models constructed, the two structures most consistent with the EXAFS data were the $(Co_2H_9)^{5-}$ and $(Co_2H_{12})^{8-}$ structures.

Time dependent DFT calculations were performed in order to simulate the Co K-edge pre-edge and edge regions using ORCA v. 2.9. Geometries from above were utilized. The B3LYP functional and def2-tzvp(-f) basis set was utilized. As core level transitions were examined, we made use of the ZORA approximation to account for relativistic effects. Because TD-DFT over-estimates transition energies, all transitions were required a red-shift of 271.4 eV. Transition intensities were normalized such that the simulated pre-edge peak for the $(Co_2H_9)^{5-}$ complex matched the experimental data. Individual transitions were convolved into Gaussian peaks and summed (line width set equal to 1.5 eV). These were then added to a sigmoidal function describing the edge jump.

XANES Simulations:

XANES simulations were performed as follows. A large number of Co_2H_9 and Co_2H_{12} core structures with two MgBr units about the core were generated. The models assumed mirror plane symmetry down the bridging hydride plane of the molecule. Hydrides were grouped into bridging and terminal hydrides. Structures were then generated using a Monte Carlo type scheme where the Co-Co core was allowed to vary between 2.3 – 2.6 Å, the terminal hydride Co-H bond lengths were allowed to vary between 1.4 – 1.6 Å, the bridging hydride Co-H bond lengths were allowed to vary between 1.7 – 1.9 Å, the Co-Mg bond lengths allowed to vary between 2.8 – 3.8 Å, and the Br-Mg bond lengths allowed to vary between 1.8 – 2.8 Å. The XANES of each structure was simulated using FEFF 9.0, and the data compared to the simulation using a simple least square analysis (see below for simulation parameters used). Differences in energies between the spectra and simulation were accounted for by blue-shifting the simulated data such simulated and experimental spectra maxima occurred at identical energies. Once a best fit to the gross

structure of the Co-cluster was obtained, the model was further refined through minor alteration in bond lengths with no symmetry restraints until a best fit was obtained (RMS of the bond length displacement was < 0.002 Å; maximum bond length displacement < 0.004 Å).

The XANES calculations within FEFF 9.0 utilized a fine grid (xkmax = 6, xkstep = 0.05 and vixan = 0.3), and the full multiple scattering card (FMS; rfms = 15.0; default parameters for all other arguments). They took advantage of FEFF's self-consistent potential calculation (SCF; rfms1 = 15.0 and all other values set to FEFF defaults), the RSIGMA card, NLEG set to 2, and local density of states calculations (LDOS; emin = –30, emax = 20, eimag = 0.1). The DEBEY card was used with the temperature set to 70 K and the Debye temperature set to 100 K (there is no theoretical justification for these parameters, it has been our experience that these work best for simulations of XANES data collected on crystallographically defined first-row transition metal complexes obtained at 20 – 30 K on this beamline by simple trial and error) and the correlated-Debye method was used. All other default FEFF parameters were used in the simulations.

Table S-1. Structural data for triply hydrogen-bridged binuclear metal complexes

Compound	M-M Distance	experiment	reference
$[Co_2(\mu_3\text{-}H_3)(\eta^5\text{-}C_5Me_5)_2]$	2.253(9)	neutron diffraction	10
$[Co_2(\mu_3\text{-}H_3)(\eta^5\text{-}C_5H_2(^t\text{Bu})_3)_2]$	2.275(21)	neutron diffraction	11
$[Co_2(\mu_3\text{-}H_3)(H)(\text{dippp})_2]$	2.2841	X-ray diffraction	12
$[Co_2(\mu_3\text{-}H_3)(as_3)_2]^+$	2.377(8)	X-ray diffraction	13
$[(CoH_3)_2(\mu_3\text{-}H_3)]^{5-}$	2.452(2)	EXAFS	this work
$[Ir_2(\mu_3\text{-}H_3)(\eta^5\text{-}Cp^*)_2]^+$	2.465(3)	neutron diffraction	14
$[Re_2(\mu_3\text{-}H_3)H_6\ (\text{triphos})]^-$	2.594(1)	neutron diffraction	15
$[Ti(^t\text{Bu-L})\}_2(\mu_3\text{-}H_3)]^{3-}$	2.6210 (10)	X-ray diffraction	16

Table S-2. Alternate Models for the EXAFS data to $Co_2H_n^{m-}$.

	Co-Co	Co-H(1)	Co-H(2)	Co-Mg	Co-Br
Model 1 n r (Å) σ^2 (Å^2) $\varepsilon^2 = 0.82$	1 2.4238(14) 0.00255(11)	N/A	N/A	N/A	N/A
Model 2 n r (Å) σ^2 (Å^2) $\varepsilon^2 = 0.78$	1 2.4487(3) 0.0026(2)	8(2) 1.822(13) 0.009(5)	N/A	N/A	N/A
Model 3 n r (Å) σ^2 (Å^2) $\varepsilon^2 = 0.73$	1 2.4487(11) 0.00273(9)	4(1) 1.543(3) 0.0031(2)	2(1) 1.823(3) 0.0009(15)	N/A	N/A
Model 4 n r (Å) σ^2 (Å^2) $\varepsilon^2 = 0.68$	1 2.451(2) 0.0027(3)	4(1) 1.541(4) 0.0033(2)	2(1) 1.822(5) 0.0012(8)	1 3.61(5) 0.009(17)	1 4.87(8) 0.011(22)

Table S-2. XYZ coordinates for the final optimized XANES model.

Co	-3.62681	0.52227	0.25592
H	-2.66874	1.61842	-0.60969
H	-4.43925	-0.51451	1.11887
H	-4.89724	1.40427	0.54689
H	-4.60968	-0.00447	-0.85524
H	-0.17371	1.06711	-1.04065
Co	-1.23412	1.13256	0.12189
H	-2.08662	-0.43621	0.00797
H	-0.46359	2.48511	0.36234
H	-2.40054	1.07063	1.50279
H	-0.00805	0.56518	0.92747
Mg	-6.53589	-0.09459	0.41364
Mg	1.64712	2.08224	0.38087
Br	-7.67619	-1.16067	1.11160
Br	2.89326	3.24606	-0.38104

Table S-3. XYZ coordinates for the mPWPW91 geometry optimized $(Co_2H_9)^{5-}$ model.

Co	-3.592249	0.484770	0.303225
H	-2.667465	1.614497	-0.615074
H	-4.404686	-0.552011	1.166175
H	-4.862679	1.366763	0.594199
H	-4.575117	-0.041974	-0.807936
H	-0.240647	0.947375	-0.913150
Co	-1.301055	1.012832	0.249397
H	-2.173005	-0.455510	0.007969
H	-0.530520	2.365378	0.489842
H	-2.486920	1.051333	1.502786
H	-0.074985	0.445449	1.054976

Table S-4. XYZ coordinates for the mPWPW91 geometry optimized $(Co_2H_{12})^{8-}$ model.

Co	-3.63643	0.12777	0.32488
H	-2.92869	-1.14482	0.82135
H	-2.49103	0.53500	-0.96476
H	-4.56961	-0.17938	1.39603
H	-4.09530	1.58026	0.56092
H	-3.96451	-1.06628	-0.50832
H	-4.69622	0.50055	-0.65584
H	-0.41409	1.39742	-0.96988
H	-2.04576	2.37551	-0.38294
Co	-1.34871	1.09124	0.10066
H	-0.90114	-0.36200	-0.14759
H	-0.99752	2.27479	0.93947
H	-2.49859	0.70003	1.38726
H	-0.29225	0.69711	1.07783

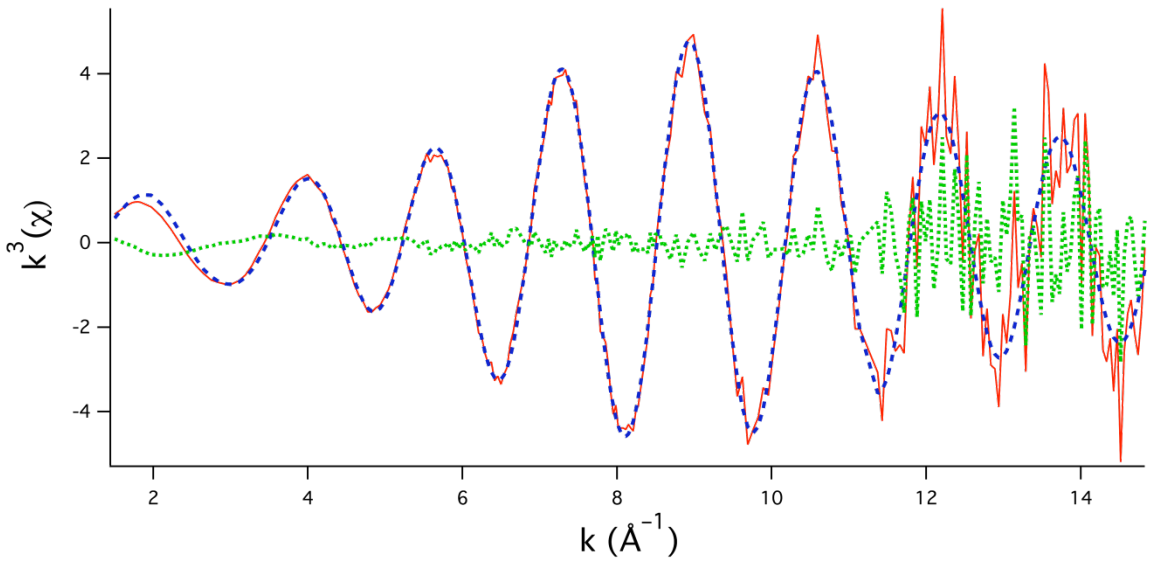

Figure S-1. Unfiltered $k^3(\chi)$ EXAFS spectra depicting the experimental data (red), simulated data (blue dashed; model 4) and difference spectrum (green dotted line).

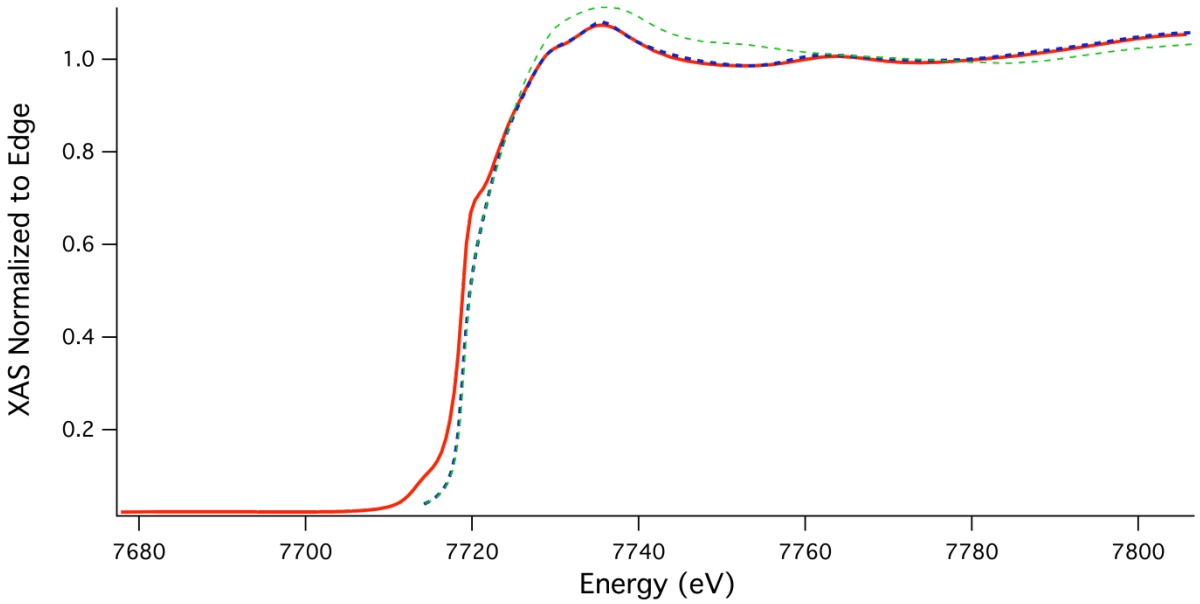

Figure S-2. Best fit to the XANES data (red) with the Co_2H_9 (blue) vs. Co_2H_{12} (green) models.

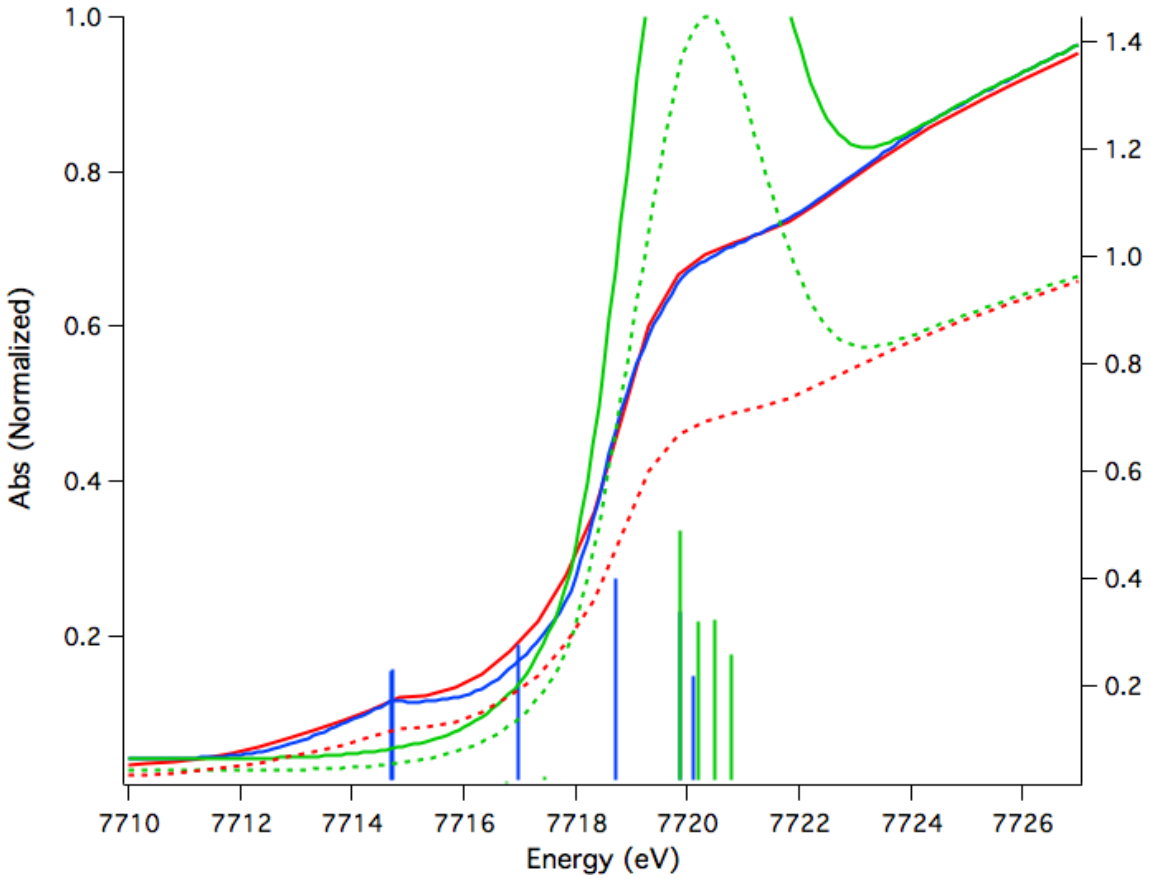

Figure S-3. Simulations of the pre-edge region using TD-DFT. The red spectrum represents the experimental data. Solid spectra correspond to the left y-axis while dashed spectra correspond to the right y-axis. The blue and green spectra are the convolutions of the pre-edge transitions determined from the TD-DFT calculations and a sigmoidal function representing the edge jump. The blue spectrum is from the $(Co_2H_9)^{5-}$ complex while the green spectrum is for the $(Co_2H_{12})^{8-}$ complex. The blue [$(Co_2H_9)^{5-}$) and green $(Co_2H_{12})^{8-}$] sticks represent the individual transitions. The individual transitions for $(Co_2H_9)^{5-}$ were multiplied five-fold for clarity in the figure.

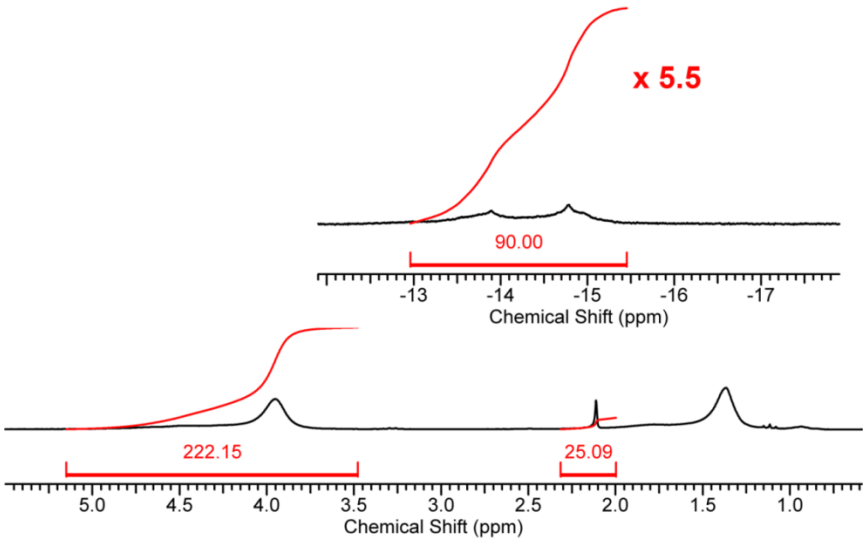

Fig. S-4. ^{1}H NMR spectra of (**1**) taken in assorted solutions in C_6D_6. **(a)** (**1**) 3 mg/mL

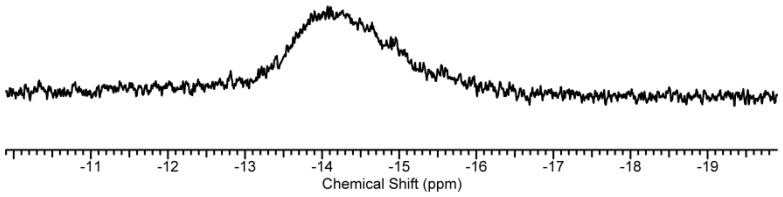

(b) Hydride region of (**1**) with 10 equiv. of HMPA in C_6D_6

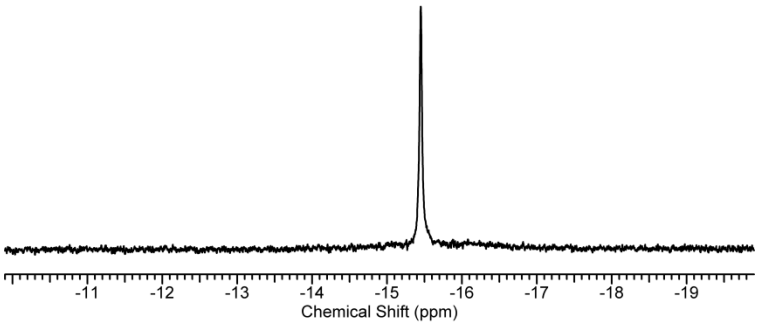

(c) Hydride region of (**1**) with ca. 10 equiv. [$MgBr_2(THF)_2$] in C_6D_6

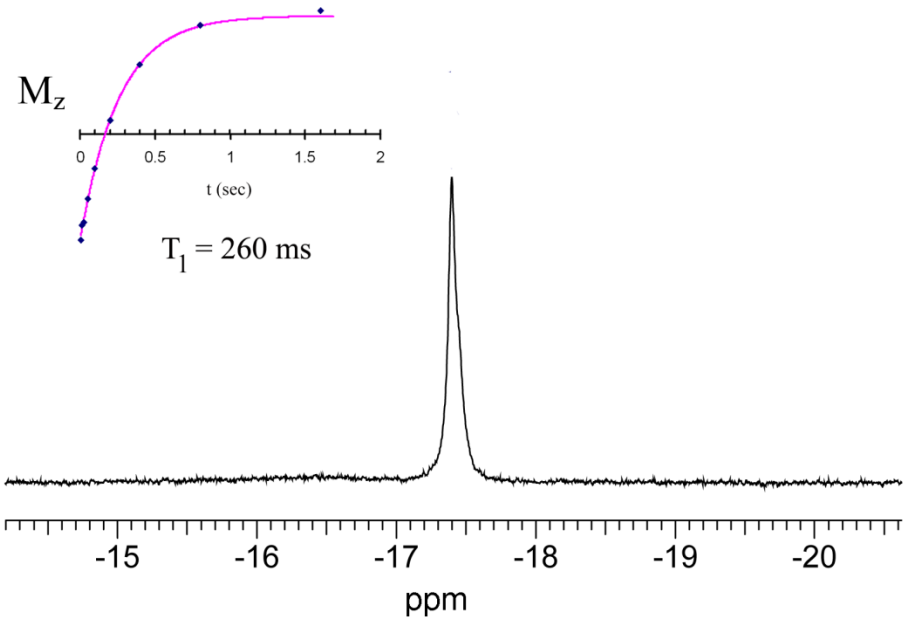

Fig. S-5. ^{1}H NMR measurement for (**1**) (0.004 M) in [$MgBr_2(THF)_2$]-doped (0.02 M) THF-d_8 showing the hydride region with inset of 180-τ-90 determination of T_1 for the Co-H resonance

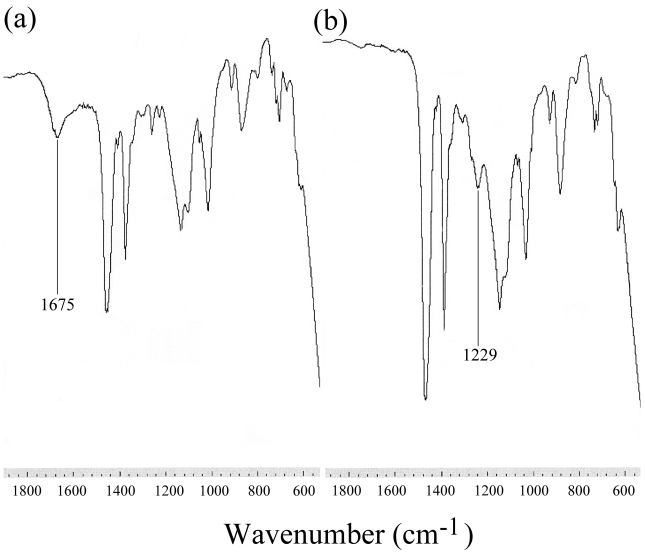

Fig. S-6. IR spectra (Nujol) of (**1**) (a) and its d_9-isotopomer (b) presented on scales of %T 0-50% and 0-70%, respectively.

References

1. D. E. Linn, Jr., G. M. Skidd and E. M. Tippmann, *Inorg. Chim. Acta*, 1999, **291**, 142-147.

2. D. E. Linn, Jr., G. M. Skidd and S. N. McVay, *Inorg. Chem*., 2002, **41**, 5320-5322

3. ACD NMR Processor, Advanced Chemistry Development, Inc., Toronto, On, Canada, www.acdlabs.com, 2013.

4. D. A. Skoog, D. M. West, F. J. Holler, Fundamentals of Analytical Chemistry, 7th ed., 1996, Harcourt Brace, New York, 829-831.

5. Knovel Critical Tables, 2nd Edition, 2008, http://www.knovel.com/, accessed August 12, 2013.

6. Shearer, J.; Scarrow, R.S. *EXAFS123: A software package for the work-up, analysis and plotting of X-ray Absorption Data*. University of Nevada, Reno (2007).

7. a) Shearer, J.; Soh, P. *Inorg. Chem.* **2007**, *46*, 710-719. b) Scarrow, R.C.; Brennan, B.A; Cummings, J.G.; Jin, H.; Duong, D.J.; Kindt, J.T.; Nelson, M.J. *Biochemistry*, **1996**, *35*, 10078-10088. c) Scarrow, R.C.; Strickler, B.S.; Ellison, J.J.; Shoner, S.C.; Kovacs, J.A.; Cummings, J.G.; Nelson, M.J. *J. Am. Chem. Soc.* **1998**, *120*, 9237-9245.

8. Rehr, J.J.; Kas, J.J.; Vila, F.D.; Prange, M.P.; Jorissen, K. *Phys. Chem. Chem. Phys.* **2010**, *12*, 5503-5513.

9. Neese, F. *Wiley Interdisciplinary Reviews: Computational Molecular Science* **2012**, *2*, 73-78.

10. F. Lutz, R. Bau, P. Wu, T. F. Koetzle, C. Krüger and J. J. Schneider, *Inorg. Chem*., 1996, **35**, 2698.

11. M. Bortz, *J. Clust. Sci.*, 2001, 1, 285.

12. M. Fryzuk, J. Ng, S. Rettig, J. Huffman, K. Jonas, Inorg. Chem., 1991, 30, 2437-2441.

13. P. Daporto, S. Mindollini, L. Sacconi, *Inorg. Chem*., 1975, **14**, 1643.

14. R. C. Stebens, M. R. McLean, T. Wen, J. D. Carpemter, R. Bau, T. F. Koetzle, *Inorg. Chim Acta*, 1989, **161**, 223.

15. S. C. Abrahams, A. P. Ginsberg, T. F. Koetzle, P. Marsh, C. R. Sprinkel, *Inorg. Chem*., 1986, **25**, 2500.

16. T. Matsuo, H. Kawaguchi, *Organometallics*, 2003, **22**, 5379-5381.